Hybrid light-matter states in topological superconductors coupled to cavity photons

Olesia Dmytruk [1,2] and Marco Schirò [2]

[1] *CPHT, CNRS, École Polytechnique, Institut Polytechnique de Paris, 91120 Palaiseau, France*

[2] *JEIP, UAR 3573 CNRS, Collège de France, PSL Research University, 11 Place Marcelin Berthelot, 75321 Paris Cedex 05, France*

(Received 10 October 2023; revised 28 May 2024; accepted 23 July 2024; published 13 August 2024)

We consider a one-dimensional topological superconductor hosting Majorana bound states at its ends coupled to a single mode cavity. In the strong light-matter coupling regime, electronic and photonic degrees of freedom hybridize resulting in the formation of polaritons. We find the polariton spectrum by calculating the cavity photon spectral function of the coupled electron-photon system. In the topological phase, the lower in energy polariton modes are formed by the bulk-Majorana transitions coupled to cavity photons and are also sensitive to the Majorana parity. In the trivial phase, the lower polariton modes emerge due to the coupling of the bulk-bulk transitions across the gap to photons. Our work demonstrates the formation of polaritons in topological superconductors coupled to photons that contain information on the features of the Majorana bound states.

DOI: 10.1103/PhysRevB.110.075416

I. INTRODUCTION

Cavity embedding provides a promising avenue to probe and control quantum materials and devices. On the one hand there is the tantalizing possibility of controlling phase transitions and phase diagrams by coupling to a cavity mode, an idea which has received theoretical and experimental attention [1,2]. Another source of cavity control can arise from the hybridization with finite-frequency modes, leading to new hybrid quasiparticles—polaritons [3], which can be then probed and controlled in novel ways. A wide range of polaritonic modes have been proposed and observed, classified depending on the type of charged particles in the matter component [4].

A particularly appealing scenario arises when the material has a nontrivial topological character, a feature which can then be enhanced or suppressed [5–11] or even generated by the coupling with a cavity and thus transmitted to the emergent polariton excitations [12]. Among topological phases of matter, topological superconductors hosting zero-energy Majorana bound states [13–16] hold a specially interesting place for their potential for quantum computing [17]. The prototype system for topological superconductivity is the Kitaev chain model [13] describing a one-dimensional p-wave superconductor with Majorana bound states emerging at its opposite ends in the topological phase. Promising platforms for the Majorana bound states are superconductor-semiconductor nanowires [18,19], graphenelike systems [20,21], and chains of magnetic atoms [22–24]. Signatures of the Majorana bound states in the form of zero-bias peak have been experimentally observed in superconductor-semiconductor nanowire platforms [25–31]. However, theoretical works have demonstrated that the zero-bias peak could arise due to non-Majorana mechanisms [32–40].

The idea of using cavities to probe and manipulate the Majorana bound states has been explored in different settings [41–49]. In these cases, the cavity plays mainly the role of noninvasive spectroscopic tool to probe the physics of these modes. A different scenario arises potentially in the strong or ultrastrong light-matter coupling regime where polariton modes are formed, which in the case of a topological superconductor could take the form of the Majorana polaritons [50,51].

In this work, we study the hybrid light-matter states that emerge by coupling topological superconductors to a single mode cavity. We consider two models of topological superconductors hosting the Majorana bound states: a prototype Kitaev chain model [13] and a more realistic nanowire model [18,19]. Hybridization between electronic and photonic states results in formation of polaritons. We focus specifically on the signatures of these polaritonic modes which emerge in the cavity photon spectral function [9,52–55], which is directly measurable in a transmission/reflection experiment [42,56]. We find that the polariton spectrum is sensitive to the Majorana parity in the topological phase. Moreover, the energies of the polariton modes are different in the trivial and topological phases that could be used to probe the emergence of zero modes in topological superconductor.

The paper is organized as follows. In Sec. II, we introduce two tight-binding models for topological superconductors and derive how to couple them to a single mode cavity. Then, in Sec. III, we calculate the polariton spectrum of the coupled electron-photon system. Finally, Sec. IV is devoted to conclusions.

II. COUPLING TOPOLOGICAL SUPERCONDUCTORS TO LIGHT

We start by discussing how to couple topological superconductors described by a tight-binding model to a single mode cavity. We consider two models for topological superconductors: (1) a prototype Kitaev chain [13] and (2) an experimentally relevant nanowire with spin-orbit interaction and proximity-induced superconductivity subject to magnetic field [18,19]. Contrary to previously studied tight-binding models for nonsuperconducting systems [9,54], the Kitaev chain (nanowire) models contain p-wave (s-wave)

superconducting pairing term that pairs two neighboring sites (opposite spins) in the chain.

A. Kitaev chain coupled to cavity

The Hamiltonian for the Kitaev chain reads [13]

$$H_K = -\mu \sum_{j=1}^{N} c_j^\dagger c_j - t \sum_{j=1}^{N-1} (c_j^\dagger c_{j+1} + \text{H.c.}) + \Delta \sum_{j=1}^{N-1} (c_j c_{j+1} + \text{H.c.}), \quad (1)$$

where $c_j^\dagger$ (c_j) are fermionic creation (annihilation) operators at site j, N is the total number of sites in the chain, μ is the chemical potential, t is the hopping amplitude, and Δ is a p-wave superconducting pairing potential. The Kitaev chain is in the topological (trivial) phase if $|\mu| < 2t$ ($|\mu| > 2t$) hosting two Majorana bound states described by the operators $\gamma_{L(R)} = \gamma_{L(R)}^\dagger$. These two Majorana operators form a full fermionic state with $c_M = (\gamma_L - i\gamma_R)/2$ that gives rise to the Majorana occupation $n_M = \langle c_M^\dagger c_M \rangle$ that determines its parity. The Majorana occupation n_M can be 0 or 1 corresponding to the even (odd) parity.

Next, we couple the Kitaev chain to a single mode cavity given by the Hamiltonian $H_{ph} = \omega_c(a^\dagger a + 1/2)$, where $a^\dagger$ (a) is the photonic creation (annihilation) operator and ω_c is the cavity frequency. The Kitaev chain Hamiltonian H_K is coupled to the electromagnetic field described by a homogeneous photonic vector potential $\mathbf{A} = \mathbf{u}_x(g/e)(a + a^\dagger)$ via the Peierls substitution, which is equivalent to applying a unitary transformation U to the electronic Hamiltonian (6) only [9,54], $H_{K-ph} = H_{ph} + U^\dagger H_K U$, with

$$U = e^{i\frac{g}{\sqrt{N}}(a+a^\dagger)\sum_j R_j c_j^\dagger c_j}. \quad (2)$$

Here, $R_j = j - l_0$, where $l_0 = (N+1)/2$ chosen such that $R_1 = -R_N$. Using that

$$U^\dagger c_m U = e^{i\frac{g}{\sqrt{N}}(a+a^\dagger)R_m} c_m, \quad (3)$$

we find that the superconducting pairing term acquires a site-dependent phase and the full light-matter Hamiltonian reads

$$H_{K-ph} = -\mu \sum_{j=1}^{N} c_j^\dagger c_j - \sum_{j=1}^{N-1} \left(t e^{i\frac{g}{\sqrt{N}}(a+a^\dagger)} c_j^\dagger c_{j+1} + \text{H.c.} \right) + \sum_{j=1}^{N-1} \left(\Delta e^{i\frac{g}{\sqrt{N}}(2R_j+1)(a+a^\dagger)} c_j c_{j+1} + \text{H.c.} \right) + \omega_c \left(a^\dagger a + \frac{1}{2} \right). \quad (4)$$

Moreover, we note that coupling the superconducting pairing term to light is equivalent to dressing Δ with a phase, $\Delta \to \Delta e^{i\varphi}$ [43,57,58]. The phase φ could be found under the assumption that the p-wave pairing term in H_K is inherited from the bulk s-wave superconductor underneath the wire. In this case, we consider that the instantaneous supercurrent flowing through the bulk superconductor vanishes,

$$J_s = \frac{2e}{m} |\psi|^2 (\nabla\varphi - 2e\mathbf{A}) \equiv 0. \quad (5)$$

Here, m, $|\psi|^2$, and φ are the electronic mass, the density of superconducting electrons in the s-wave superconductor, and its phase, respectively. The solution of the differential equation $\nabla\varphi = 2e\mathbf{A}$ gives us $\varphi_j = 2g(a + a^\dagger)(j - l_0 + 1/2)\sqrt{N}$. Here, φ_j is chosen such that $\varphi_1 = -\varphi_{N-1}$ [56]. We note that these two approaches result in the same light-matter Hamiltonian given by Eq. (4). Alternatively, light-matter coupling could be included in the problem by starting with a semiconducting nanowire tunnel coupled to a bulk s-wave superconductor and assuming that the tunneling hopping is dressed with the Peierls phase [42].

B. Superconductor-semiconductor nanowire coupled to cavity

We now consider a more realistic model of a topological superconductor coupled to a photonic cavity. The tight-binding Hamiltonian composed of N sites that describes a semiconducting nanowire with Rashba spin-orbit interaction and proximity-induced superconductivity subject to magnetic field reads [59]

$$H_{nw} = \sum_{j,\sigma,\sigma'} \Big[c_{j+1,\sigma}^\dagger (-t\delta_{\sigma\sigma'} + i\alpha\sigma_{\sigma\sigma'}^y) c_{j,\sigma'} + \Delta c_{j,\uparrow}^\dagger c_{j,\downarrow}^\dagger + \frac{1}{2} c_{j,\sigma}^\dagger [(2t - \mu)\delta_{\sigma\sigma'} + V_Z \sigma_{\sigma\sigma'}^x] c_{j,\sigma'} + \text{H.c.} \Big], \quad (6)$$

where $c_{j,\sigma}^\dagger$ ($c_{j,\sigma}$) is the creation (annihilation) operator acting on electrons with spin σ located at site j, $\sigma_{x(y)}$ is the x (y) Pauli matrix acting in the spin space, and $t = \hbar^2/(2m^* a_l^2)$ is the hopping amplitude, with m^* the effective mass and a_l lattice constant. Here, α is the spin-orbit coupling, Δ is the proximity-induced superconducting pairing potential, μ is the chemical potential, and $V_Z = g^* \mu_B B/2$ is the Zeeman energy, with g^* the g-factor of the nanowire and μ_B the Bohr magneton. The nanowire hosts Majorana bound states emerging at the opposite ends of the one-dimensional system if $V_Z > \sqrt{\Delta^2 + \mu^2}$ [18,19].

Similarly to the Kitaev chain, the light-matter Hamiltonian for the nanowire coupled to a single mode cavity could be obtained by performing the unitary transformation $H_{nw-ph} = H_{ph} + U^\dagger H_{nw} U$, with

$$U = e^{i\frac{g}{\sqrt{N}}(a+a^\dagger)\sum_{j\sigma} \chi_j c_{j\sigma}^\dagger c_{j\sigma}}. \quad (7)$$

Here, $\chi_j = j - j_0$ is chosen such that $\chi_1 = -\chi_N$ [56], with $j_0 = (N+1)/2$ for even N. Using that

$$U^\dagger c_{m\sigma'} U = e^{i\frac{g}{\sqrt{N}}(a+a^\dagger)\chi_m} c_{m\sigma'}, \quad (8)$$

we find that total light-matter coupling Hamiltonian becomes

$$H_{nw-ph} = \sum_{j,\sigma,\sigma'} \Big[c_{j+1,\sigma}^\dagger \big(-t e^{-i\frac{g}{\sqrt{N}}(a+a^\dagger)} \delta_{\sigma\sigma'} + i\alpha e^{-i\frac{g}{\sqrt{N}}(a+a^\dagger)} \sigma_{\sigma\sigma'}^y \big) c_{j,\sigma'} + \Delta e^{-2i\frac{g}{\sqrt{N}}\chi_j(a+a^\dagger)} c_{j,\uparrow}^\dagger c_{j,\downarrow}^\dagger$$

$$+\frac{1}{2}c^{\dagger}_{j,\sigma}[(2t-\mu)\delta_{\sigma\sigma'}+V_Z\sigma^x_{\sigma\sigma'}]c_{j,\sigma'}+\text{H.c.}\Big]$$
$$+\omega_c\left(a^{\dagger}a+\frac{1}{2}\right). \tag{9}$$

In the next section, we will discuss the cavity photon spectral function for the two models in Eqs. (4) and (9) and highlight the emergence of polariton excitations and their topological signatures.

III. POLARITON SPECTRUM

In the strong light-matter coupling regime, the electronic and photonic degrees of freedom get entangled and hybridize giving rise to polaritons, new hybrid excitations of mixed light-matter character. In conventional cavity-QED systems, such as for the example in the prototypical Dicke model [60–62], the cavity couples to a collective matter excitation and the resulting theory can be described in a harmonic approximation, from which polariton spectrum follows from direct diagonalization of coupled bosonic modes. In the solid-state context of interest here the cavity couples to many electronic modes through a highly nonlinear Peierls phase, such that a direct diagonalization of the polariton spectrum cannot be obtained. An alternative way to access the polariton spectrum is however by looking at the cavity photonic spectral function, defined as

$$A(\omega)=-\frac{1}{\pi}\text{Im}\int dt e^{-i\omega t}(-i\theta(t))\langle[a(t),a^{\dagger}]\rangle, \tag{10}$$

where $a(t)$ is the photonic annihilation operator at time t. To compute this quantity we follow Refs. [9,52–54] and write down the imaginary-time action associated to the electron-photon Hamiltonian from which we proceed by integrating out the electronic degrees of freedom to obtain a photon-only effective problem, which we evaluate at the saddle point plus Gaussian fluctuations in the cavity field (see Appendix A for more details). Due to gauge invariance, the photon remains incoherent in presence of a uniform vector potential [54, 63–66]. The light-matter coupling however gives rise to a self-energy correction for the cavity spectral function arising from current-current fluctuations of the electronic system. As a result the cavity spectral function takes the form [9,54]

$$A(\omega)=-\frac{1}{\pi}\frac{\chi''(\omega)(\omega+\omega_c)^2}{(\omega^2-\omega_c^2-2\omega_c\chi'(\omega))^2+(2\omega_c\chi''(\omega))^2}, \tag{11}$$

where $\chi(\omega)=K(\omega)-\langle J_d\rangle\equiv\chi'(\omega)+i\chi''(\omega)$ is the current-current correlation function that can be separated into real $\chi'(\omega)$ and imaginary $\chi''(\omega)$ parts, with

$$K(t-t')=-i\theta(t-t')\langle[J_p(t),J_p(t')]\rangle. \tag{12}$$

Here, J_p (J_d) are paramagnetic (diamagnetic) current operators that could be defined from the second-order expansion in g [9,54]

$$H_{K(nw)-ph}\approx\omega_c a^{\dagger}a+H_{K(nw)}+(a+a^{\dagger})J_p-\frac{(a+a^{\dagger})^2}{2}J_d \tag{13}$$

and $\theta(t-t')$ is the Heaviside step function. We see that Eq. (11) describes the spectrum of single particle excitations in the photonic sector and in absence of any light-matter coupling it reduces to a sharp delta-function at the cavity frequency. Due to light-matter coupling we see from the above expression that the cavity mode acquires a renormalization to its frequency and a finite lifetime, both effects being due to the electronic self-energy correction $\chi(\omega)$. The poles of the cavity spectral functions $A(\omega)$, given by the solutions of the equation [54,65]

$$\omega^2\approx\omega_c^2+2\omega_c\chi'(\omega). \tag{14}$$

give direct access to the excitations of the coupled system, which as mentioned describe polaritons. In Refs. [9,54], we had shown indeed that for cases in which the polariton spectrum could be computed by diagonalising an effective bosonic problem, the identification with the poles of the photonic spectral function is meaningful and captures the essential physics. This is ultimately because the cavity mode retains a finite overlap with the polariton excitations.

Going back to Eq. (11), we see that for $g=0$ the topological superconductor and cavity photons are fully decoupled and there is a single solution of Eq. (14) given by $\omega=\omega_c$. For finite light-matter coupling $g\neq 0$, electrons and photons are coupled resulting in multiple solutions that depend both on cavity frequency ω_c and parameters of the electronic system through the real part of the current-current correlation function $\chi'(\omega)$. Therefore the resulting polariton energies are sensitive to the properties of the topological superconductor.

A. Current-current correlation function

We start by deriving the general expression for the current-current correlation function $\chi(\omega)$. Coupling between topological superconductor and cavity photons induces transitions between the Majorana and bulk states in the chain [42,48,49]. These Majorana-bulk transitions could be directly seen as peaks in the imaginary part of the correlation function $K(\omega)$ Eq. (12). To evaluate $K(\omega)$, we rewrite the fermionic operators c_j ($c_j^{\dagger}$) in terms of the annihilation (creation) operators $\tilde{c}_n$ ($\tilde{c}_n^{\dagger}$) for the Bogoliubov quasiparticles [42,48]

$$c_j=\sum_n(u_{j,n}\tilde{c}_n+v_{j,n}\tilde{c}_n^{\dagger}), \tag{15}$$

so that the electronic Hamiltonian (1) (6) becomes diagonal $\tilde{H}_{el}=\sum_n\epsilon_n(\tilde{c}_n^{\dagger}\tilde{c}_n-1/2)$. Here, $u_{j,n}$ ($v_{j,n}$) are the electron (hole) components of the eigenvectors and ϵ_n are the corresponding eigenvalues of the electronic Hamiltonian, with $n=1,\ldots,N$ for the Kitaev chain Hamiltonian (1) and $n=1,\ldots,2N$ for the superconductor-semiconductor nanowire Hamiltonian (6). To calculate the expectation value of the diamagnetic current operator $\langle J_d\rangle$ over a bare electronic Hamiltonian (1) (6) we rewrite J_d in terms of $\tilde{c}_n$ ($\tilde{c}_n^{\dagger}$) operators and use that $\langle\tilde{c}_n^{\dagger}\tilde{c}_m\rangle=f(\epsilon_n)\delta_{n,m}$, with $f(\epsilon_m)$ being the Fermi distribution function. Assuming zero temperature, $f(\epsilon_m)$ reduces to the occupation number n_m that can take values 0 or 1 for empty or occupied state. Under this assumption, we arrive

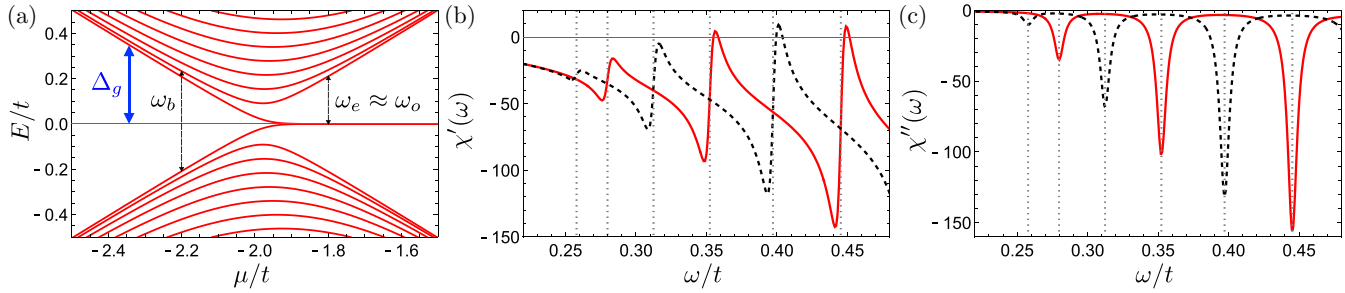

FIG. 1. (a) Energy spectrum of the Kitaev chain (1) as a function of the chemical potential μ/t (red solid lines). Vertical blue solid arrow indicates the effective gap in the energy spectrum Δ_g. Vertical black dashed arrows indicate the transition frequencies ω_b and $\omega_{e(o)}$. For the chosen set of parameters Majorana energy $\epsilon_M/t = 7.44 \times 10^{-7}$ and $\omega_e \approx \omega_o \approx \Delta_g$. (b) Real part of the current-current correlation function $\chi'(\omega)$ as a function of frequency ω/t. Red solid (black dashed) lines correspond to even (odd) Majorana parity. The transition frequencies ω_e are shown in gray vertical dotted lines. (c) Imaginary part of the current-current correlation function $\chi''(\omega)$ as a function of frequency ω/t for even (odd) Majorana parity shown in red solid (black dashed) lines. Gray vertical dotted lines correspond to the transition frequencies and indicate the position of the peaks. Parameters are chosen as $N = 100$, $\Delta/t = 1$, $\mu/t = -1.75$ [except in (a)], $\eta/t = 4 \times 10^{-3}$.

at the following expression:

$$\langle J_d \rangle = \sum_m j_m^d n_m, \tag{16}$$

where j_m^d is the diagonal matrix element for the diamagnetic current operator between eigenstates corresponding to the eigenvalues ϵ_m. Defining the Fourier transformation as $K(\omega) = \int e^{i\omega t} K(t)$ and using that $\tilde{c}_m(t) = \tilde{c}_m(0)e^{-i\epsilon_m t}$, we find the general expression for the paramagnetic current correlation function at zero temperature

$$K(\omega) = \sum_{l,m} \left| j_{l,m}^p \right|^2 \frac{n_l - n_m}{\omega + \epsilon_l - \epsilon_m + i\eta}. \tag{17}$$

Here, $j_{l,m}^p$ are the matrix elements of the paramagnetic current and $\eta > 0$ is the linewidth of the energy levels. While Eq. (17) is general, here for the sake of clarity we make explicit reference to the spectrum of the Kitaev model and its current-current correlation function depicted in Fig. 1.

At zero temperature, only bulk states with negative energies are occupied, while $n_l \equiv n_M = 0, 1$ for the Majorana states. We note that $K(\omega) = 0$ for $l = m$ making it fully off-diagonal in contrast to $\langle J_d \rangle$. When the system is in the topological phase the paramagnetic current correlation function given by Eq. (17) can be rewritten as a sum of three contributions $K(\omega) = K_{BB}(\omega) + K_{BM}(\omega) + K_{MM}(\omega)$, corresponding respectively to transitions between bulk states only (K_{BB}), between Majorana and bulk states (K_{BM}) and between Majorana states only (K_{MM}) [see Fig. 1(a)]. We note that $K_{MM}(\omega) = 0$ since Majorana parity remains conserved in the presence of coupling to photons [42]. The bulk only contribution in the topological phase (or the total paramagnetic current correlation function in the trivial phase) could be further simplified to

$$K_{BB}(\omega) = \sum_{\epsilon_{l\neq m}>0} \left(\frac{1}{\omega - \omega_b + i\eta} - \frac{1}{\omega + \omega_b + i\eta} \right) \times \left| j_{l,-m}^p \right|^2, \tag{18}$$

where $\omega_b = \epsilon_l + \epsilon_m$ is the transition frequency between the bulk states l and m, and $j_{l,-m}^p$ is the matrix element between the bulk states with energies ϵ_l and $-\epsilon_m$. The peaks in the imaginary part of the bulk contribution appear at transition frequencies $\omega_b > 2\Delta_g$, where Δ_g is the effective gap in the electronic energy spectrum [see Fig. 1(a)].

Furthermore, the bulk-Majorana transitions are included in $K_{BM}(\omega)$ term given by

$$K_{BM}(\omega) = \sum_{\epsilon_l>0} \left(\frac{1}{\omega - \omega_{e(0)} + i\eta} - \frac{1}{\omega + \omega_{e(0)} + i\eta} \right) \times \left[\left| j_{l,o}^p \right|^2 (n_M - n_l) + \left| j_{l,e}^p \right|^2 (1 - n_l - n_M) \right], \tag{19}$$

where $\omega_{e(0)} = \epsilon_l \pm \epsilon_M$ is the transition frequency between bulk state with occupation number $n_l = 0$ and Majorana state with occupation number $n_M = 0(1)$ corresponding to even (odd) parity, and $j_{l,e(o)}^p$ is the matrix element between bulk state l and even e (odd o) parity Majorana state. The imaginary part of the paramagnetic current correlation function $K''_{BM}(\omega)$ calculated for even parity with $n_M = 0$ has multiple peaks at frequency $\omega_e > \Delta_g$ with the amplitude given by $|j_{l,e}^p|^2$, while for $n_M = 1$ the peaks are at ω_o with the amplitude given by $|j_{l,o}^p|^2$ [see Fig. 1(c)]. Moreover, even in the absence of the overlap between two Majorana bound states $\epsilon_M \approx 0$ the correlation function $K_{BM}(\omega)$ distinguishes between different Majorana parities through the matrix elements $j_{l,e(o)}^p$ [48].

In the topological phase the cavity spectral function $A(\omega)$ given by Eq. (11) depends on the Majorana parity through the different matrix elements entering in the current-current correlation function $\chi(\omega)$ and, therefore, polariton spectrum could be used to probe Majorana properties. Comparing the denominators in Eqs. (19) and (18) we note that the lowest-energy peaks in the current-current correlation function in the topological [shown in Figs. 1(b) and 1(c)] and trivial phases appear at frequencies $\omega_{e(o)} \approx \Delta_g$ and $\omega_b \approx 2\Delta_g$, respectively, suggesting that the cavity spectral function could be also used to differentiate between two phases, as we are going to discuss next for the two specific models of interest.

B. Polaritons in Kitaev chain coupled to photons

We start discussing the cavity spectral function for the Kitaev chain, Eq. (4). In this case, the paramagnetic and

diamagnetic current operators could be found from Eq. (4):

$$J_p = i\frac{g}{\sqrt{N}}\sum_j[-tc_j^\dagger c_{j+1} + 2\Delta(R_j + 1/2)c_j c_{j+1} - \text{H.c.}] \tag{20}$$

and

$$J_d = \frac{g^2}{N}\sum_j[-tc_j^\dagger c_{j+1} + 4\Delta(R_j + 1/2)^2 c_j c_{j+1} + \text{H.c.}], \tag{21}$$

where we see that in addition to the usual contribution from single particle hopping there is also a term coming from the superconducting pairing. We emphasize that this current is not associated with a conserved charge in the Kitaev model, which only enjoys a discrete Z_2 parity symmetry. However, it is the natural object entering the response of the system to the cavity vector potential, see Eq. (13).

To find the cavity spectral function we first calculate the current-current correlation function using Eqs. (16) and (17). In Fig. 1(b), we plot the real part of correlation function $\chi'(\omega)$ as a function of frequency ω. Vertical dotted lines indicate the bulk-Majorana transition frequencies $\omega_{e(o)}$. For the Kitaev chain in the topological phase, $\epsilon_M \approx 0$ and therefore $\omega_e \approx \omega_o$. We find that $\chi'(\omega)$ has different oscillation amplitudes for even and odd Majorana parities stemming from the difference in the matrix elements $j^p_{l,e}$. Next, we numerically evaluate the imaginary part of the correlation function $\chi''(\omega)$ [see Fig. 1(c)]. The function $\chi''(\omega)$ has multiple peaks at resonant frequencies $\omega_{e(o)}$ that differ for two parities, similarly to the features present in $\chi'(\omega)$. Therefore the current-current correlation function $\chi(\omega)$ is a good marker to distinguish between two Majorana parities in the topological phase.

Given the above results for the current-current correlator we can now focus on the cavity photon spectral function (11). We plot $A(\omega)$ as a function of frequency in Fig. 2(a) at a fixed light-matter coupling g for different parities in the topological phase. The current-current correlation function is calculated for a finite-length Kitaev chain and has many resonances [see Fig. 1(b)], therefore, Eq. (14) has multiple solutions for polariton energies corresponding to peaks in $A(\omega)$. Moreover, the polariton spectrum in the topological phase depends on the Majorana parity through $\chi'(\omega)$. The cavity spectral function has different patterns for two parities and can distinguish between the parities. We further compute the cavity spectral function in the trivial phase [see Fig. 2(b)] for the same light-matter coupling strength g and the effective gap Δ_g. We find that $A(\omega)$ has a sharp peak around the cavity frequency ω_c as in the topologically nontrivial phase. However, we note that contrary to the topological case small peaks emerge at frequencies larger than $2\Delta_g$ corresponding to bulk-bulk transition across the gap in the system.

In Fig. 3(a), we plot the cavity spectral function for the Kitaev chain in the topological phase as a function of frequency and light-matter coupling. We consider a cavity frequency in resonance with the first bulk-Majorana transition for the even parity ($\omega_c = \omega_e$). We see that for low frequency there is a broad peak which shifts towards lower frequencies upon increasing g. At higher frequencies, on the other hand, we recognize sharp features associated with transitions between

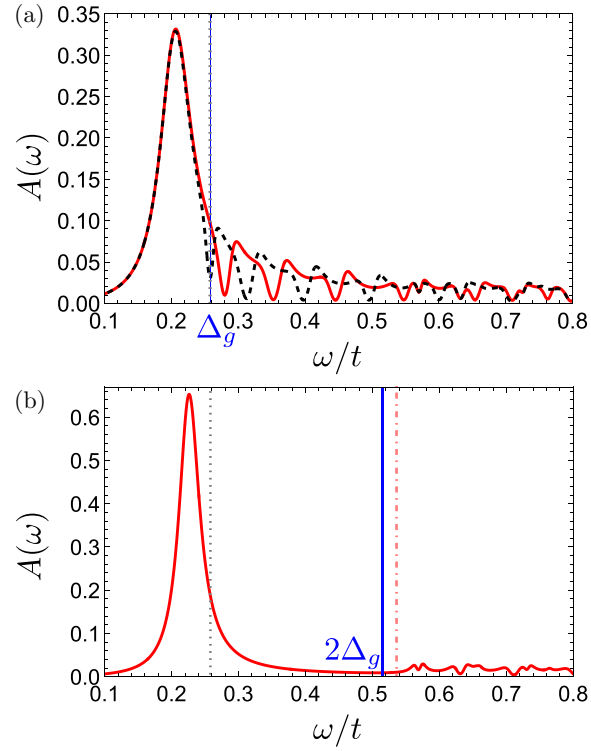

FIG. 2. Cavity spectral function $A(\omega)$ as a function of frequency ω/t for $g = 0.1$. (a) In the topological phase ($\mu/t = -1.75$), the red solid (black dashed) line corresponds to even (odd) Majorana parity. The vertical gray dotted line indicates the cavity frequency $\omega_c = \omega_e$ fixed to be in resonance with the first bulk-Majorana transition. The vertical blue solid line indicates the effective gap in the Kitaev chain spectrum $\Delta_g \approx \omega_e$ ($\epsilon_M/t = 7.44 \times 10^{-7}$). (b) In the trivial phase ($\mu/t = -2.25$), there is a large peak that emerges at ω_c (vertical gray dotted line) for $g = 0$ and shifts to smaller frequencies at finite g. Smaller peaks appear at frequencies larger than $2\Delta_g$ shown in vertical blue solid line. The pink dot-dashed line indicates the first bulk-bulk transition at frequency $\omega_b > 2\Delta_g$. Other parameters are the same as in Fig. 1.

Majorana and bulk states. Next, we calculate $A(\omega)$ for the Kitaev chain in the trivial phase [see Fig. 3(b)]. As discussed for the topological phase there is a broad peak that originates at $\omega = \omega_c$ for $g = 0$ and further broadens as the light-matter coupling strength is increased. However, in the trivial phase, the current-current correlation function $\chi(\omega)$ that enters Eq. (11) has resonances only at frequencies $\omega_b > 2\Delta_g$. Therefore other polariton modes appear only at $\omega > 2\Delta_g$. Comparing the cavity spectral function calculated in the topological phases we note the distinct features between the two, namely that the sharp features of the transitions between Majorana (bulk)-bulk states appear at different energy scales of Δ_g ($2\Delta_g$). Therefore the polariton spectrum could be potentially used as a way to probe zero-energy states in topological superconductors.

C. Polaritons in nanowire coupled to photons

We now move to the superconductor-semiconductor nanowire model, Eq. (9), for which the paramagnetic and

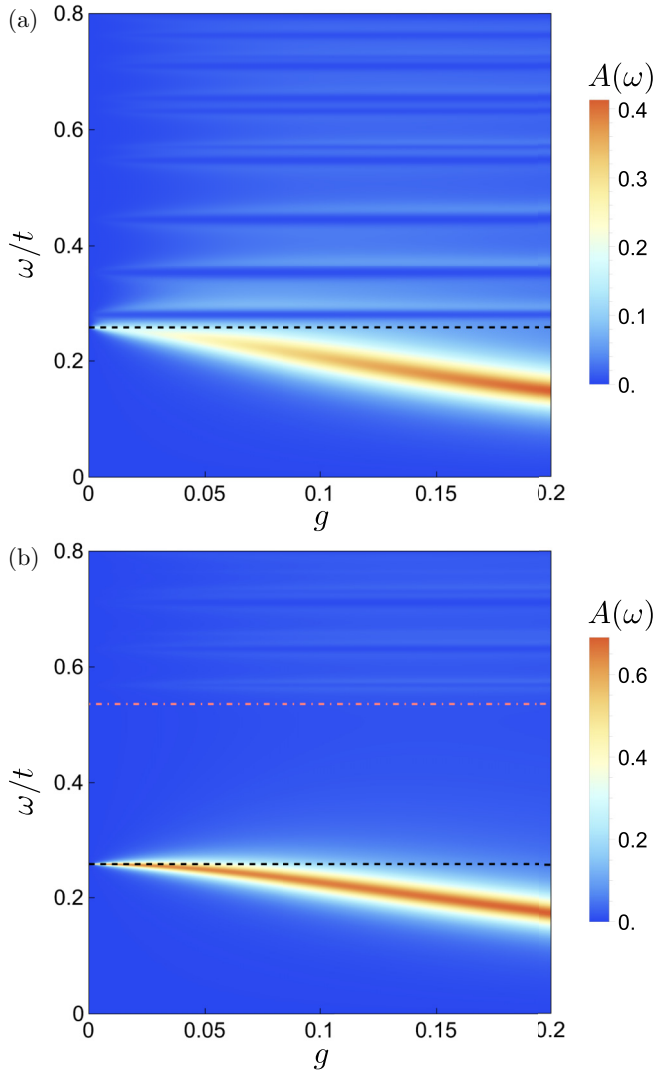

FIG. 3. Spectral function $A(\omega)$ as a function of g and ω/t. The horizontal black dashed line corresponds to frequency ω_c chosen to be equal to first bulk-Majorana transition frequency and horizontal pink dot-dashed line corresponds to ω_b in the trivial phase. (a) In the topological phase with $\mu/t = -1.75$, the lowest polariton branch originating at $\omega = \omega_c$ for $g = 0$ goes down as g is increased. White horizontal lines corresponding to bulk-Majorana transitions coupled with photons appear at frequencies $\omega > \Delta_g$. (b) In the trivial phase with $\mu/t = -2.25$, the lowest polariton branch appears at $\omega = \omega_c$. In contrast to the topological phase, white horizontal lines correspond to bulk-bulk transitions and appear at $\omega > 2\Delta_g$. In two phases, white horizontal lines corresponding to bulk-Majorana (a) and bulk-bulk (b) transitions emerge at different frequencies signaling the presence of zero-energy states in the topological phase. Other parameters are the same as in Fig. 1.

diamagnetic current operators read respectively

$$J_p = i\frac{g}{\sqrt{N}}\sum_j [t(c^\dagger_{j+1\uparrow}c_{j\uparrow} + c^\dagger_{j+1\downarrow}c_{j\downarrow}) + \alpha(c^\dagger_{j+1\uparrow}c_{j\downarrow} - c^\dagger_{j+1\downarrow}c_{j\uparrow}) - 2\Delta\chi_j c^\dagger_{j\uparrow}c^\dagger_{j\downarrow} - \text{H.c.}] \quad (22)$$

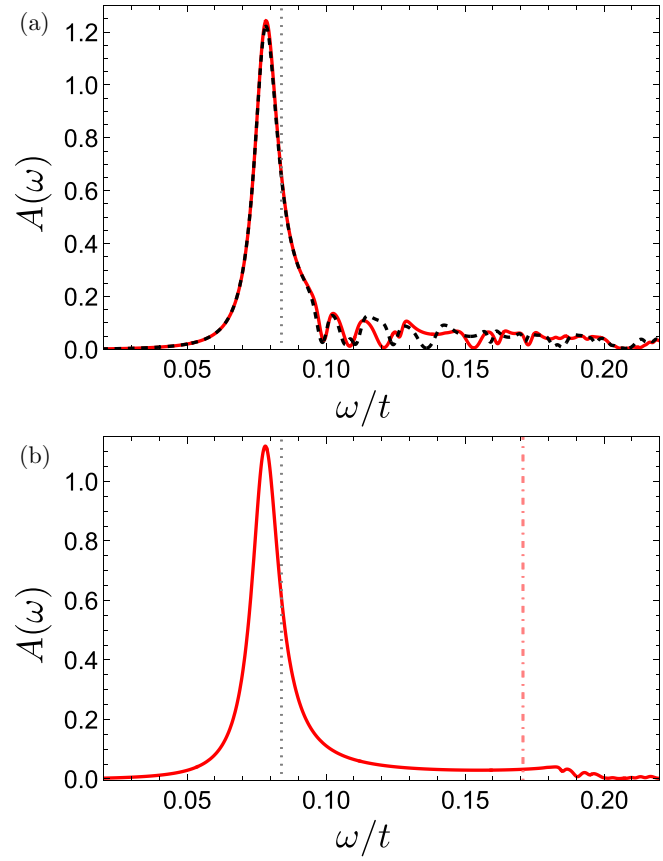

FIG. 4. Cavity spectral function $A(\omega)$ of the nanowire as a function of frequency ω/t for light-matter coupling strength $g = 0.05$. (a) Red solid (black dashed) lines correspond to $n_M = 0$ ($n_M = 1$) in the topological phase with $V_Z/\Delta = 1.8$. The gray vertical dotted line indicates the cavity frequency ω_c resonant with the first bulk-Majorana transition at $\omega_e \approx \omega_o$ ($\epsilon_M/t = 10^{-6}$). (b) $A(\omega)$ for the nanowire in the trivial phase with $V_Z/\Delta = 0.2$. The vertical gray dotted line indicates ω_c and pink dot-dashed line signals the position of the first bulk-bulk transition frequency ω_b. Other parameters are fixed as $N = 100$, $\Delta/t = 0.1$, $\mu = 0$, $\alpha/t = 0.4$, and $\eta/t = 10^{-3}$.

and

$$J_d = \frac{g^2}{N}\sum_j [-t(c^\dagger_{j+1\uparrow}c_{j\uparrow} + c^\dagger_{j+1\downarrow}c_{j\downarrow}) + \alpha(c^\dagger_{j+1\uparrow}c_{j\downarrow} - c^\dagger_{j+1\downarrow}c_{j\uparrow}) + 4\Delta\chi_j^2 c^\dagger_{j\uparrow}c^\dagger_{j\downarrow} + \text{H.c.}]. \quad (23)$$

To find the cavity spectral function of the nanowire model, we proceed in the same way as for the Kitaev chain. The real and imaginary part of $\chi(\omega)$ has similar structure to Fig. 1, but the position and amplitude of the peaks are less homogeneous due to more involved energy spectrum of the nanowire.

In Fig. 4, we plot the cavity spectral function for the nanowire model as a function of frequency ω for a fixed value of the light-matter coupling g. In the topological phase, we consider different parities depicted in solid red and black dashed lines in the absence of the Majorana overlap, with $\epsilon_M/t = 10^{-6}$. Moreover, in the presence of the Majorana overlap, the dependence of $A(\omega)$ on the Majorana parity becomes

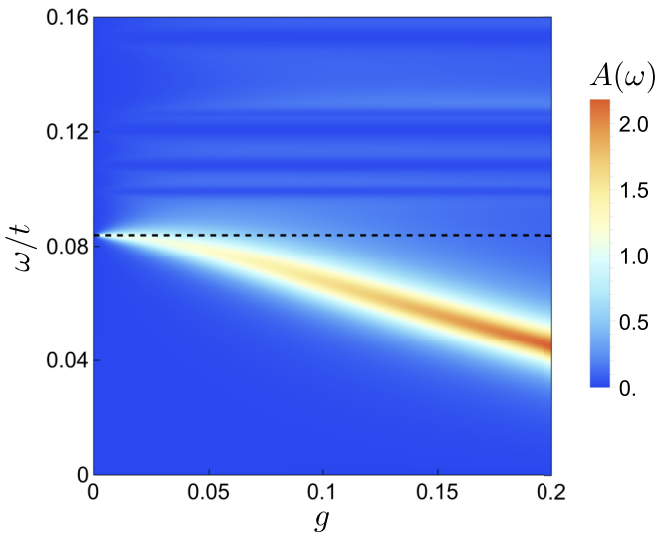

FIG. 5. Cavity spectral function $A(\omega)$ of the nanowire as a function of the light-matter coupling g and frequency ω/t. The black dashed line indicates the value of cavity frequency $\omega_c = \omega_e$ (resonant with the first bulk-Majorana transition for even parity). White horizontal lines correspond to bulk-Majorana transitions and emerge at frequencies $\omega > \Delta_g$. Other parameters are the same as in Fig. 4.

even more pronounced, see Appendix B. The cavity spectral function has a large peak around the cavity frequency ω_c resonant with the lowest bulk-Majorana transition frequency $\omega_e \approx \omega_o$ and multiple smaller peaks corresponding to higher in energy bulk-Majorana transitions appearing at $\omega > \Delta_g$ [see Fig. 4(a)]. Considering the superconductor-semiconductor nanowire in the trivial phase coupled to photonic cavity, we find that the cavity spectral function has a sharp peak originating at the frequency ω_c and multiple smaller peaks at frequencies $\omega > 2\Delta_g$ that stem from the bulk-bulk transitions in the nanowire [see Fig. 4(b)]. Similar features were found for the Kitaev chain [see Fig. 2(b)] and allow one to probe the presence of zero-energy modes in the topological superconductor.

Finally, we present $A(\omega)$ for the nanowire in the topological phase as a function of frequency and light-matter coupling strength in Fig. 5. By choosing the cavity frequency to be equal to the first bulk-Majorana transition frequency, we find the appearance of a broad low-frequency polariton mode that goes down in ω with increasing g. Higher-frequency polariton modes appear due to coupling between higher bulk-Majorana transitions and photons showing a dense pattern of modes. Similar behavior was found for the Kitaev chain (see Fig. 3).

IV. CONCLUSIONS

In this work, we studied a one-dimensional topological superconductor coupled to cavity photons. We calculated the cavity spectral function of the electron-photon system that revealed the polariton spectrum of the hybrid system. The peaks in cavity spectral function appear at different energy scales for the electronic chain in the trivial and topological phase. Moreover, in the topological phase associated with the presence of the Majorana bound states the polariton spectrum has a different pattern for two Majorana parities. While the peaks in the cavity spectral function appearing at low energies could be attributed to non-Majorana zero energy states, the dependence on the Majorana parity remains a unique property of a topological superconductor. We note that our findings could be generalized to 2D and 3D topological systems hosting Majorana bound states. The dependence of the polariton spectrum on the Majorana parity stems from the bulk-Majorana transitions that are also present in a 3D system and could be used to probe Majorana parity, as was demonstrated in Ref. [49]. Therefore a cavity spectral function could be used to probe topological properties of the electronic chain.

ACKNOWLEDGMENTS

O.D. acknowledges helpful discussions with Jelena Klinovaja, Daniel Loss, Pascal Simon, and Mircea Trif. This project has received funding from the European Union's Horizon 2020 research and innovation programme under the Marie Skłodowska-Curie Grant Agreement No. 892800. This project has received funding from the European Research Council (ERC) under the European Union's Horizon 2020 research and innovation programme (Grant Agreement No. 101002955 - CONQUER).

APPENDIX A: DERIVATION OF CAVITY SPECTRAL FUNCTION

In this section, we provide details on the derivation of the expression (11) for the cavity spectral function. Following Refs. [9,52–54], we write down the action corresponding to the topological superconductor coupled to cavity, $S = S_{\text{el}} + S_{\text{el-ph}} + S_{\text{ph}}$, with S_{el} containing only electronic fields, $S_{\text{el-ph}}$ describing the electron-photon coupling part, and

$$S_{\text{ph}} = -\int_0^\beta d\tau d\tau' \phi^*(\tau) d_0^{-1}(\tau - \tau')\phi(\tau'). \tag{A1}$$

Here, $(\phi^*(\tau), \phi(\tau))$ are the photonic fields at the imaginary time τ and $d_0^{-1}(\tau - \tau') = -\delta(\tau - \tau')(\partial_\tau + \omega_c)$ is the bare photon Green's function.

In order to obtain the cavity spectral function, we first derive a cavity-only effective action by integrating out the electronic degrees of freedom. This can be done by rewriting the partition function of the topological superconductor coupled to cavity $Z = \int \mathcal{D}[\phi, \phi^*, C, C^*]e^{-S}$ as

$$Z = \int \mathcal{D}[\phi, \phi^*]e^{-S_{\text{eff}}} \equiv \int \mathcal{D}[\phi, \phi^*]e^{-(S_{\text{ph}} - \ln Z_0)}, \tag{A2}$$

where

$$Z_0[\phi, \phi^*] = \int \mathcal{D}[C, C^*]e^{-S_{el}[C,C^*] - S_{\text{el-ph}}[\phi,\phi^*,C,C^*]}. \tag{A3}$$

By expanding the effective action to second order in photonic fields $\phi(\tau)$, we obtain

$$\tilde{S}_{\text{eff}} = \frac{1}{2}\int d\tau d\tau' \Phi^\dagger(\tau)\left[\mathcal{D}_0^{-1}(\tau - \tau') - \Pi(\tau - \tau')\right]\Phi(\tau'), \tag{A4}$$

where $\mathcal{D}_0^{-1}(\tau - \tau')$ is the bare photon Green's function written in the Nambu basis $\Phi^\dagger(\tau) = (\phi^*(\tau), \phi(\tau))$, and

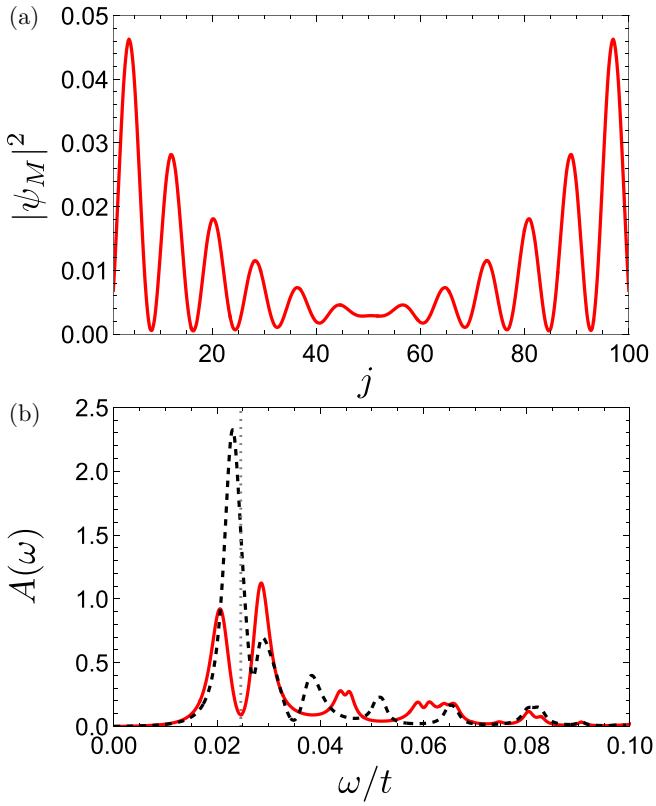

FIG. 6. (a) The Majorana probability density $|\psi_M|^2$ as a function of the lattice site j. Majorana bound states overlap resulting in the finite Majorana energy $\epsilon_M/t = 0.002$. (b) Cavity spectral function $A(\omega)$ of the nanowire as a function of frequency ω/t for light-matter coupling strength $g = 0.05$. Red solid (black dashed) lines correspond to the Majorana parity $n_M = 0$ ($n_M = 1$). Gray vertical dotted line indicates the cavity frequency ω_c resonant with the first bulk-Majorana transition at $\omega_e/t = 0.025$. Other parameters are fixed as $N = 100$, $V_Z/\Delta = 1.77$, $\Delta/t = 0.1$, $\mu = 0$, $\alpha/t = 0.04$, and $\eta/t = 10^{-3}$.

$\Pi(\tau - \tau')$ is the polarization given by

$$\Pi(\tau - \tau') = \left(\begin{array}{cc} \frac{\delta^2 \ln Z_0[\Phi,\Phi^*]}{\delta\phi^*(\tau)\delta\phi(\tau')} & \frac{\delta^2 \ln Z_0[\Phi,\Phi^*]}{\delta\phi^*(\tau)\delta\phi^*(\tau')} \\ \frac{\delta^2 \ln Z_0[\Phi,\Phi^*]}{\delta\phi(\tau)\delta\phi(\tau')} & \frac{\delta^2 \ln Z_0[\Phi,\Phi^*]}{\delta\phi(\tau)\delta\phi^*(\tau')} \end{array} \right) \Bigg|_{\Phi=0}. \quad \text{(A5)}$$

From the above equation for the effective action one can immediately read off the cavity Green's function $\mathcal{D}^{-1}(\tau - \tau') = \mathcal{D}_0^{-1}(\tau - \tau') - \Pi(\tau - \tau')$ from which the spectral function given in the main text follows after analytic continuation. We note that all four components of the polarization are equal to $\chi(\omega)$ defined in the main text.

APPENDIX B: CAVITY SPECTRAL FUNCTION FOR OVERLAPPING MAJORANA BOUND STATES

In this section, we consider the case of overlapping Majorana bound states in the nanowire model coupled to a single mode cavity (9). We plot the Majorana probability density at the lattice site j in Fig. 6(a). Two Majorana bound states are no longer localized at the opposite ends of the nanowire and overlap with each other along the nanowire length. This overlap of the wave functions gives rise to the finite energy splitting between two Majorana bound states, $\epsilon_M/t = 0.002$. We note that the transition frequencies for even and odd Majorana parities are no longer equal, $\omega_e \neq \omega_o$. We first calculate the cavity spectral function for overlapping Majorana bound states at a fixed value of the light-matter coupling strength g [see Fig. 6(b)]. We find that the dependence of $A(\omega)$ on the Majorana parity n_M becomes even more pronounced in the presence of the Majorana overlap compared to nonoverlapping case shown in Fig. 4(a).

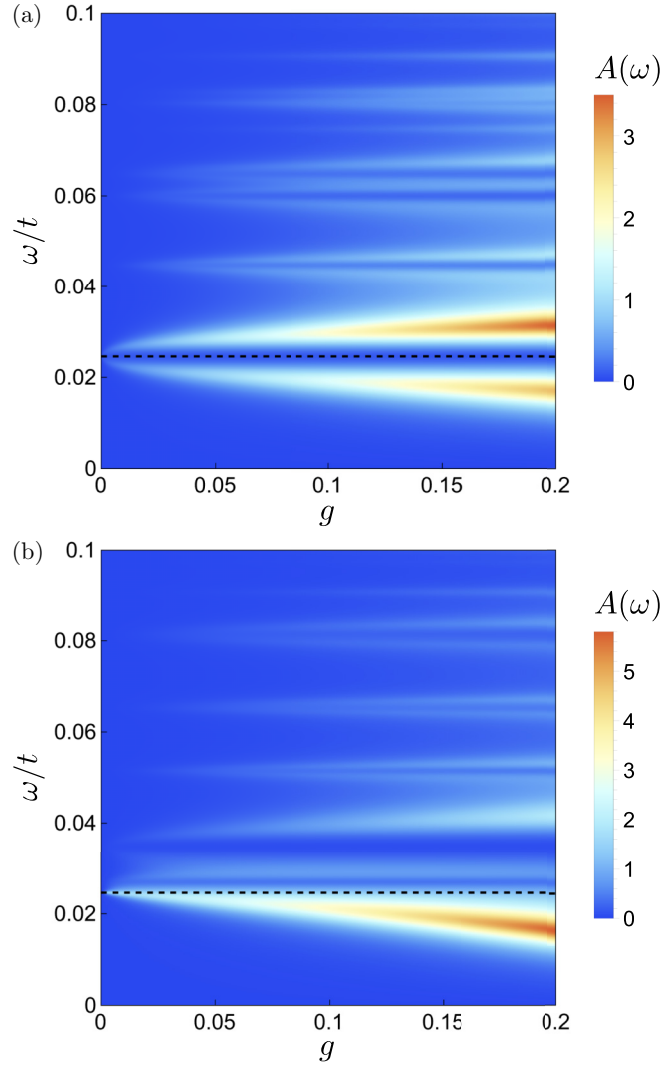

FIG. 7. Cavity spectral function $A(\omega)$ of the nanowire as a function of the light-matter coupling g and frequency ω/t. Horizontal black dashed line indicates the value of cavity frequency $\omega_c/t = \omega_e/t = 0.025$ (resonant with the first bulk-Majorana transition for even parity). Majorana bound states overlap resulting in the finite Majorana energy $\epsilon_M/t = 0.002$. (a) $A(\omega)$ for even Majorana parity. (b) $A(\omega)$ for odd Majorana parity. Other parameters are fixed as $N = 100$, $V_Z/\Delta = 1.77$, $\Delta/t = 0.1$, $\mu = 0$, $\alpha/t = 0.04$, and $\eta/t = 10^{-3}$.

In Fig. 7, we plot the cavity spectral function for the nanowire in the topological phase as a function of frequency and light-matter coupling for even [panel (a)] and odd [panel (b)] Majorana parities. The amplitude and position of the peaks in the cavity spectral function is different for two parities.

[1] F. J. Garcia-Vidal, C. Ciuti, and T. W. Ebbesen, Manipulating matter by strong coupling to vacuum fields, Science **373**, eabd0336 (2021).

[2] F. Schlawin, D. M. Kennes, and M. A. Sentef, Cavity quantum materials, Appl. Phys. Rev. **9**, 011312 (2022).

[3] J. J. Hopfield, Theory of the contribution of excitons to the complex dielectric constant of crystals, Phys. Rev. **112**, 1555 (1958).

[4] D. N. Basov, A. Asenjo-Garcia, P. J. Schuck, X. Zhu, and A. Rubio, Polariton panorama, Nanophotonics **10**, 549 (2021).

[5] C. Ciuti, Cavity-mediated electron hopping in disordered quantum hall systems, Phys. Rev. B **104**, 155307 (2021).

[6] D.-P. Nguyen, G. Arwas, Z. Lin, W. Yao, and C. Ciuti, Electron-photon chern number in cavity-embedded 2D moiré materials, Phys. Rev. Lett. **131**, 176602 (2023).

[7] D.-P. Nguyen, G. Arwas, and C. Ciuti, Electron conductance of a cavity-embedded topological 1D chain, arXiv:2402.19244 [cond-mat.mes-hall].

[8] F. Appugliese, J. Enkner, G. L. Paravicini-Bagliani, M. Beck, C. Reichl, W. Wegscheider, G. Scalari, C. Ciuti, and J. Faist, Breakdown of topological protection by cavity vacuum fields in the integer quantum Hall effect, Science **375**, 1030 (2022).

[9] O. Dmytruk and M. Schirò, Controlling topological phases of matter with quantum light, Commun. Phys. **5**, 271 (2022).

[10] B. Pérez-González, G. Platero, and Álvaro Gómez-León, Light-matter correlations in quantum Floquet engineering, arXiv:2302.12290 [cond-mat.mes-hall].

[11] D. Shaffer, M. Claassen, A. Srivastava, and L. H. Santos, Entanglement and topology in Su-Schrieffer-Heeger cavity quantum electrodynamics, Phys. Rev. B **109**, 155160 (2024).

[12] T. Karzig, C.-E. Bardyn, N. H. Lindner, and G. Refael, Topological polaritons, Phys. Rev. X **5**, 031001 (2015).

[13] A. Y. Kitaev, Unpaired Majorana fermions in quantum wires, Phys. Usp. **44**, 131 (2001).

[14] J. Alicea, New directions in the pursuit of Majorana fermions in solid state systems, Rep. Prog. Phys. **75**, 076501 (2012).

[15] C. Beenakker, Search for Majorana fermions in superconductors, Annu. Rev. Condens. Matter Phys. **4**, 113 (2013).

[16] E. Prada, P. San-Jose, M. W. A. de Moor, A. Geresdi, E. J. H. Lee, J. Klinovaja, D. Loss, J. Nygård, R. Aguado, and L. P. Kouwenhoven, From Andreev to Majorana bound states in hybrid superconductor–semiconductor nanowires, Nat. Rev. Phys. **2**, 575 (2020).

[17] S. D. Sarma, M. Freedman, and C. Nayak, Majorana zero modes and topological quantum computation, npj Quantum Inf. **1**, 15001 (2015).

[18] R. M. Lutchyn, J. D. Sau, and S. Das Sarma, Majorana fermions and a topological phase transition in semiconductor-superconductor heterostructures, Phys. Rev. Lett. **105**, 077001 (2010).

[19] Y. Oreg, G. Refael, and F. von Oppen, Helical liquids and Majorana bound states in quantum wires, Phys. Rev. Lett. **105**, 177002 (2010).

[20] C. Dutreix, M. Guigou, D. Chevallier, and C. Bena, Majorana fermions in honeycomb lattices, Eur. Phys. J. B **87**, 296 (2014).

[21] P. San-Jose, J. L. Lado, R. Aguado, F. Guinea, and J. Fernández-Rossier, Majorana zero modes in graphene, Phys. Rev. X **5**, 041042 (2015).

[22] S. Nadj-Perge, I. K. Drozdov, B. A. Bernevig, and A. Yazdani, Proposal for realizing Majorana fermions in chains of magnetic atoms on a superconductor, Phys. Rev. B **88**, 020407(R) (2013).

[23] J. Klinovaja, P. Stano, A. Yazdani, and D. Loss, Topological superconductivity and Majorana fermions in RKKY systems, Phys. Rev. Lett. **111**, 186805 (2013).

[24] B. Braunecker and P. Simon, Interplay between classical magnetic moments and superconductivity in quantum one-dimensional conductors: Toward a self-sustained topological Majorana phase, Phys. Rev. Lett. **111**, 147202 (2013).

[25] V. Mourik, K. Zuo, S. M. Frolov, S. R. Plissard, E. P. A. M. Bakkers, and L. P. Kouwenhoven, Signatures of Majorana fermions in hybrid superconductor-semiconductor nanowire devices, Science **336**, 1003 (2012).

[26] M. T. Deng, C. L. Yu, G. Y. Huang, M. Larsson, P. Caroff, and H. Q. Xu, Anomalous zero-bias conductance peak in a Nb-InSb nanowire-Nb hybrid device, Nano Lett. **12**, 6414 (2012).

[27] A. Das, Y. Ronen, Y. Most, Y. Oreg, M. Heiblum, and H. Shtrikman, Zero-bias peaks and splitting in an Al–InAs nanowire topological superconductor as a signature of Majorana fermions, Nat. Phys. **8**, 887 (2012).

[28] H. O. H. Churchill, V. Fatemi, K. Grove-Rasmussen, M. T. Deng, P. Caroff, H. Q. Xu, and C. M. Marcus, Superconductor-nanowire devices from tunneling to the multichannel regime: Zero-bias oscillations and magnetoconductance crossover, Phys. Rev. B **87**, 241401(R) (2013).

[29] M. T. Deng, S. Vaitiekėnas, E. B. Hansen, J. Danon, M. Leijnse, K. Flensberg, J. Nygård, P. Krogstrup, and C. M. Marcus, Majorana bound state in a coupled quantum-dot hybrid-nanowire system, Science **354**, 1557 (2016).

[30] M. W. A. de Moor, J. D. S. Bommer, D. Xu, G. W. Winkler, A. E. Antipov, A. Bargerbos, G. Wang, N. van Loo, R. L. M. O. het Veld, S. Gazibegovic, D. Car, J. A. Logan, M. Pendharkar, J. S. Lee, E. P. A. M. Bakkers, C. J. Palmstrøm, R. M. Lutchyn, L. P. Kouwenhoven, and H. Zhang, Electric field tunable superconductor-semiconductor coupling in Majorana nanowires, New J. Phys. **20**, 103049 (2018).

[31] M. Aghaee, A. Akkala, Z. Alam, R. Ali, A. Alcaraz Ramirez, M. Andrzejczuk, A. E. Antipov, P. Aseev, M. Astafev, B. Bauer *et al.* (Microsoft Quantum), InAs-Al hybrid devices passing the topological gap protocol, Phys. Rev. B **107**, 245423 (2023).

[32] G. Kells, D. Meidan, and P. W. Brouwer, Near-zero-energy end states in topologically trivial spin-orbit coupled superconducting nanowires with a smooth confinement, Phys. Rev. B **86**, 100503(R) (2012).

[33] C.-X. Liu, J. D. Sau, T. D. Stanescu, and S. Das Sarma, Andreev bound states versus Majorana bound states in quantum dot-nanowire-superconductor hybrid structures: Trivial versus topological zero-bias conductance peaks, Phys. Rev. B **96**, 075161 (2017).

[34] A. Ptok, A. Kobiałka, and T. Domański, Controlling the bound states in a quantum-dot hybrid nanowire, Phys. Rev. B **96**, 195430 (2017).

[35] F. Setiawan, C.-X. Liu, J. D. Sau, and S. Das Sarma, Electron temperature and tunnel coupling dependence of zero-bias and almost-zero-bias conductance peaks in Majorana nanowires, Phys. Rev. B **96**, 184520 (2017).

[36] C. Moore, T. D. Stanescu, and S. Tewari, Two-terminal charge tunneling: Disentangling Majorana zero modes from partially separated Andreev bound states in

semiconductor-superconductor heterostructures, Phys. Rev. B **97**, 165302 (2018).
[37] C. Reeg, O. Dmytruk, D. Chevallier, D. Loss, and J. Klinovaja, Zero-energy Andreev bound states from quantum dots in proximitized Rashba nanowires, Phys. Rev. B **98**, 245407 (2018).
[38] A. Vuik, B. Nijholt, A. R. Akhmerov, and M. Wimmer, Reproducing topological properties with quasi-Majorana states, SciPost Phys. **7**, 061 (2019).
[39] R. Hess, H. F. Legg, D. Loss, and J. Klinovaja, Local and nonlocal quantum transport due to Andreev bound states in finite Rashba nanowires with superconducting and normal sections, Phys. Rev. B **104**, 075405 (2021).
[40] R. Hess, H. F. Legg, D. Loss, and J. Klinovaja, Trivial Andreev band mimicking topological bulk gap reopening in the nonlocal conductance of long Rashba nanowires, Phys. Rev. Lett. **130**, 207001 (2023).
[41] A. Cottet, T. Kontos, and B. Douçot, Squeezing light with Majorana fermions, Phys. Rev. B **88**, 195415 (2013).
[42] O. Dmytruk, M. Trif, and P. Simon, Cavity quantum electrodynamics with mesoscopic topological superconductors, Phys. Rev. B **92**, 245432 (2015).
[43] O. Dmytruk, M. Trif, and P. Simon, Josephson effect in topological superconducting rings coupled to a microwave cavity, Phys. Rev. B **94**, 115423 (2016).
[44] M. C. Dartiailh, T. Kontos, B. Douçot, and A. Cottet, Direct cavity detection of Majorana pairs, Phys. Rev. Lett. **118**, 126803 (2017).
[45] A. Cottet, M. C. Dartiailh, M. M. Desjardins, T. Cubaynes, L. C. Contamin, M. Delbecq, J. J. Viennot, L. E. Bruhat, B. Douçot, and T. Kontos, Cavity QED with hybrid nanocircuits: From atomic-like physics to condensed matter phenomena, J. Phys.: Condens. Matter **29**, 433002 (2017).
[46] M. Trif, O. Dmytruk, H. Bouchiat, R. Aguado, and P. Simon, Dynamic current susceptibility as a probe of Majorana bound states in nanowire-based Josephson junctions, Phys. Rev. B **97**, 041415(R) (2018).
[47] M. Trif and P. Simon, Braiding of Majorana fermions in a cavity, Phys. Rev. Lett. **122**, 236803 (2019).
[48] O. Dmytruk and M. Trif, Microwave detection of gliding Majorana zero modes in nanowires, Phys. Rev. B **107**, 115418 (2023).
[49] Z. Ren, J. Copenhaver, L. Rokhinson, and J. I. Väyrynen, Microwave spectroscopy of Majorana vortex modes, Phys. Rev. B **109**, L180506 (2024).
[50] M. Trif and Y. Tserkovnyak, Resonantly tunable Majorana polariton in a microwave cavity, Phys. Rev. Lett. **109**, 257002 (2012).
[51] Z. Bacciconi, G. M. Andolina, and C. Mora, Topological protection of Majorana polaritons in a cavity, Phys. Rev. B **109**, 165434 (2024).
[52] G. Mazza and A. Georges, Superradiant quantum materials, Phys. Rev. Lett. **122**, 017401 (2019).
[53] I. Amelio, L. Korosec, I. Carusotto, and G. Mazza, Optical dressing of the electronic response of two-dimensional semiconductors in quantum and classical descriptions of cavity electrodynamics, Phys. Rev. B **104**, 235120 (2021).
[54] O. Dmytruk and M. Schiró, Gauge fixing for strongly correlated electrons coupled to quantum light, Phys. Rev. B **103**, 075131 (2021).
[55] E. Vlasiuk, V. K. Kozin, J. Klinovaja, D. Loss, I. V. Iorsh, and I. V. Tokatly, Cavity-induced charge transfer in periodic systems: Length-gauge formalism, Phys. Rev. B **108**, 085410 (2023).
[56] B. Pérez-González, Á. Gómez-León, and G. Platero, Topology detection in cavity QED, Phys. Chem. Chem. Phys. **24**, 15860 (2022).
[57] F. Pientka, A. Romito, M. Duckheim, Y. Oreg, and F. von Oppen, Signatures of topological phase transitions in mesoscopic superconducting rings, New J. Phys. **15**, 025001 (2013).
[58] A. Cottet, T. Kontos, and B. Douçot, Electron-photon coupling in mesoscopic quantum electrodynamics, Phys. Rev. B **91**, 205417 (2015).
[59] O. Dmytruk and J. Klinovaja, Suppression of the overlap between Majorana fermions by orbital magnetic effects in semiconducting-superconducting nanowires, Phys. Rev. B **97**, 155409 (2018).
[60] R. H. Dicke, Coherence in spontaneous radiation processes, Phys. Rev. **93**, 99 (1954).
[61] K. Hepp and E. H. Lieb, On the superradiant phase transition for molecules in a quantized radiation field: The dicke maser model, Ann. Phys. **76**, 360 (1973).
[62] Y. K. Wang and F. T. Hioe, Phase transition in the dicke model of superradiance, Phys. Rev. A **7**, 831 (1973).
[63] P. Nataf, T. Champel, G. Blatter, and D. M. Basko, Rashba cavity QED: A route towards the superradiant quantum phase transition, Phys. Rev. Lett. **123**, 207402 (2019).
[64] G. M. Andolina, F. M. D. Pellegrino, V. Giovannetti, A. H. MacDonald, and M. Polini, Cavity quantum electrodynamics of strongly correlated electron systems: A no-go theorem for photon condensation, Phys. Rev. B **100**, 121109(R) (2019).
[65] D. Guerci, P. Simon, and C. Mora, Superradiant phase transition in electronic systems and emergent topological phases, Phys. Rev. Lett. **125**, 257604 (2020).
[66] G. M. Andolina, F. M. D. Pellegrino, V. Giovannetti, A. H. MacDonald, and M. Polini, Theory of photon condensation in a spatially varying electromagnetic field, Phys. Rev. B **102**, 125137 (2020).